



Interaction between chlorophenols in the adsorption process on corn straw biochar

Jinkui Zhong^{a,b,*}, Wenqing Li^a, Yarui Xie^a, Ye Yang^a, Li Ding^a

^aSchool of Environmental and Municipal Engineering, Lanzhou Jiaotong University, No. 188, Anning West Road, Lanzhou 730070, China, Tel.: 86+13609343749; email: zhongjk@mail.lzjtu.cn (J. Zhong), 1760430570@qq.com (W. Li), 2142881384@qq.com (Y. Xie), 572456036@qq.com (Y. Yang), 1592785044@qq.com (L. Ding)

^bKey Laboratory of Yellow River Water Environment of Gansu Province, Lanzhou 730070, China

Received 11 October 2022; Accepted 17 February 2023

ABSTRACT

The treatment of effluents containing emerging contaminants, such as chlorophenols (CPs), by biochar adsorption has been a hotspot topic. However, the interaction between CPs in the adsorption process on biochar is still unknown at present. In this paper, two kinds of biochar were prepared from corn straw under pyrolysis of 300°C and 600°C, labeled as BC300 and BC600, respectively, and were characterized by scanning electron microscopy, X-ray photoelectron spectroscopy, and Fourier-transform infrared spectroscopy. The adsorption process and mechanism of biochar on CPs, including phenol (PHE), 4-chlorophenol (4-CP), and 2,4-dichlorophenol (2,4-DCP), were investigated using the batch equilibrium experimental method in a single component system (SCS) and multi-component system (MCS), respectively. The adsorption regularity of CPs on biochars in the MCS resembles that in the SCS. In the MCS, the pseudo-second-order kinetic model is fitted better for the adsorption process of CPs on biochar ($R^2 \geq 0.938$). The maximum adsorption capacity (q_m) of PHE, 4-CP and 2,4-DCP is 28.16, 32.54 and 36.04 mg/g, respectively. The isotherm adsorption process is fitted more consistent with Langmuir–Freundlich model ($R^2 \geq 0.913$). The q_m of PHE, 4-CP and 2,4-DCP in the MCS is 43.02, 60.85 and 96.48 mg/g, but the q_m of PHE, 4-CP and 2,4-DCP in the SCS is 63.91, 121.03 and 145.09 mg/g, respectively. The pH value of solution is a key factor influencing the adsorption of CPs on the biochar. At pH < 9, the adsorption capacity (q_e) of CPs on biochar almost remains constant as increase of pH values. By way of the contrast, at pH > 9, the q_e of CPs decreases rapidly with increasing pH values. However, there is an interaction between CPs in the adsorption process on biochar in the MCS compared with that in the SCS, that is, one or two of three co-existing pollutants can inhibit the adsorption of each of CPs on biochar. Furthermore, the adsorption capacity of CPs on biochar increases with the number of chlorine atoms in CPs, that is, the more chlorine atoms in CPs, the easier it is to be adsorbed on biochar.

Keywords: Chlorophenols; Corn straw biochar; Interaction; Adsorption

1. Introduction

The development of industry and agriculture, a new type of pollutants, called emerging contaminants (ECs), has been concerned in the world [1,2]. The chlorophenols (CPs), widely used in various industries and agricultures, are part of ECs and can get into water environment through different

ways [3,4]. The CPs possess high toxicity and bioaccumulation, so they can cause serious effects on animals and human [5,6]. Most of CPs are listed as persistent organic pollutants (POPs) due to their mutagenesis, carcinogenesis and teratogenesis [7–10].

There are physico-chemical, chemical oxidation and biological methods for the treatment for CPs, such as aerobic

* Corresponding author.

and anaerobic digestion, dechlorination, ion exchange with resin, adsorption and ozonation [11–15]. Aerobic and anaerobic digestion increases the cost of sludge treatment and consumption of chemicals [16]. Dechlorination has a large investment and complex equipment [17]. Ion exchange with resin is highly selective and short resin replacement cycle [18]. Ozonation has high operating costs and toxic gas generation [19]. Of them, the biochar adsorption method has a few advantages, such as good adsorption effect, simple adsorption process, easy operation and no secondary pollution [20,21]. Thus, the adsorption method for the treatment of wastewater containing CPs has a good potential [22–24].

The selection of adsorption materials is particularly critical for the adsorption method [25]. A few characteristics, such as high output, low cost, and no pollution, of the materials used for the adsorption of CPs are necessarily considered [26–28]. The biochars made from biomass are rich in porousness, aromaticity, hydrophobicity, and carbon element, so they are well fitted to use as adsorption materials due to high specific surface area and specific surface energy [29,30]. Thus, biochar can be used to remove the CPs in wastewater [31].

China is the largest corn straws producer in the world [32]. The corn straws, which are the major agricultural wastes, have no edible value and are often carelessly disposed [33,34]. Thus, there is a need to develop efficient ways to utilize corn straws [35]. The preparation of biochar from corn straws can improve the utilization level of straws [36]. Corn straw biochar is widely used in water treatment due to features of high adsorption capacity and wide adsorption range [37,38]. However, at present, most studies have focused on the adsorption of single phenolic or single chlorophenol compound on biochar [39,40]. A little attention has been paid to the interaction between CPs in the adsorption process due to co-existing pollutants in the real environment. In addition, the influence of the number of chlorine atoms in the CPs on its adsorption has almost not been reported.

Based on the above, different types of biochar were prepared by pyrolysis of corn straws at 300°C and 600°C, and characterized through scanning electron microscopy (SEM), Brunauer–Emmett–Teller (BET), X-ray photoelectron spectroscopy (XPS), Fourier-transform infrared spectroscopy (FTIR), specific surface area, and pore size distribution for explaining biochar adsorption characteristics on CPs. The mechanisms and interaction between CPs (PHE, 4-CP, and 2,4-DCP) in the adsorption process on biochar were

investigated. The influence of the number of chlorine atoms in the CPs on adsorption was considered. This paper can be used for the treatment of CPs in wastewater by corn straw biochar.

2. Materials and methods

2.1. Materials

The corn straws were collected from a farmland in Wushan Country, Tianshui City, Gansu Province, China. Phenol (PHE), 4-chlorophenol (4-CP), and 2,4-dichlorophenol (2,4-DCP) were purchased from Tianjin Damao Chemical Factory, China. The major physico-chemical properties of CPs are listed in Table 1.

2.2. Preparation of biochars

The corn straw was first washed with deionized water, air-dried prior to grinding to pass through a 40-mesh (0.425 mm) sieve. Then the samples of the powder biomass were pyrolyzed at 300°C and 600°C for 6 h in a muffle furnace (SX2-10-12N, China) for preparing biochar. When the temperature of the muffle furnace was cooled to ambient temperature, the biochar samples obtained were fetched out and passed through an 80-mesh sieve. The samples were subsequently washed with 1 mol/L HCl for 5 times, and then rinsed for several times with deionized water until the pH value of the liquid after washing maintained constant. The rinsed biochar was dried at 80°C in an oven, and then was passed again through the 80-mesh sieve. Finally, the samples were stored in amber bottles for subsequent use.

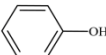
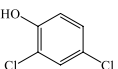
2.3. Material characterization

The surface morphology of the biochar was characterized through SEM (JSM-5600, Japan). The surface components were obtained by XPS (ESCALAB 250Xi, China). The C, H, N and O elements were determined by elemental analyzer (Vario EL, Elementar, Germany). The pore structure and specific surface area were determined by automatic physical adsorption apparatus (ASAP 2020M, USA). The nature of functional groups was analyzed by FTIR (Nexus870, USA).

2.4. Adsorption experiments

To study the interaction between CPs on corn straw biochar, and the influence of the number of chlorine atoms in

Table 1
Major physico-chemical properties of chlorophenols

Chlorophenols	Molecular formula	Molecular weight (g/mol)	Chemical structure	Solubility ^a (g/L)	pKa
Phenol	C ₆ H ₅ OH	94.11		82	9.89
4-Chlorophenol	C ₆ H ₅ ClO	128.56		25.7	9.70
2,4-Dichlorophenol	C ₆ H ₄ Cl ₂ O	163.00		4.5	7.89

^arefers to the solubility of each of chlorophenols in water at 20°C.

the CPs on the adsorption process, the batch equilibrium experiments were conducted in a 50-mL Erlenmeyer flask with stopper at 25°C.

In a single component system (SCS), only containing a single compound, each of three CPs (PHE, 4-CP, and 2,4-DCP), a fixed amount of 0.06 g BC300 or BC600 was added to the Erlenmeyer flask with 30 mL of a given concentration PHE, 4-CP, or 2,4-DCP solution. The pH value of the solution was adjusted with 0.1 mol/L HCl or 0.1 mol/L NaOH [41,42]. In the adsorption kinetics experiment and isothermal adsorption experiment, pH was adjusted to 5, and in the experiments on the effect of initial pH value, pH varied from 2 to 12.

In a multi-component system (MCS), three CPs (PHE, 4-CP, and 2,4-DCP) simultaneously co-existing in a system, a fixed amount of 0.06 g BC600 was added to a 50-mL Erlenmeyer flask with 30 mL of the CPs mixed solution. In the adsorption kinetics experiment, mixed solution containing equal parts of 70 mg/L PHE, 4-CP, and 2,4-DCP, and the pH was adjusted to 5, contact time was controlled at 0–24 h. In an isothermal adsorption experiment, each 10 mL of PHE, 4-CP, and 2,4-DCP was added to the Erlenmeyer flask, concentration ranging from 10 to 150 mg/L, and the pH was adjusted to 5. In the experiments on the effect of initial pH value, mixed solution containing equal parts of 70 mg/L PHE, 4-CP, and 2,4-DCP, initial pH values of solution varied from 2 to 12.

All tests were carried out in a gas bath thermostatic oscillation chamber (ZD-85, China) at 150 r/min. Finally, the mixed liquor was filtered through a 0.45 µm membrane for determining the concentration of CPs in the filtrates through liquid chromatography mass spectrometer (LCQ AD-40000, USA) and C18 columns (ODS HYPERSIL, 200 mm × 2.1 mm × 1.7 µm). The mobile phase was composed of methanol and water (70:30, v/v) at flow rate of 0.2 mL/min with a column temperature of 30°C. The injection volume is 5 µL by using automatic injection. The detection wavelengths for PHE, 4-CP and 2,4-DCP were set at 270, 285 and 290 nm, respectively, and the retention times were 3.03, 3.72 and 4.98 min [43].

Adsorption capacity, q_e , of CPs on biochar was calculated as Eq. (1):

$$q_e = \frac{(c_0 - c_e) \times V}{m} \quad (1)$$

where c_0 is the initial concentration of CPs (mg/L), c_e is the equilibrium concentration of CPs in the solution (mg/L), V is the volume of solution (mL), m is the mass of the biochar (g).

3. Results and discussions

3.1. Characterization

The primary physico-chemical properties of the biochars are listed in Table 2. As can be seen, before pickling, the pH values of both original BC300 and BC600 are alkaline, and the pH value of BC600 is higher than that of BC300. After pickling, the pH values of both become acidic, and the pH value of BC300 approach nearly to that of BC600 (3.69 and 3.64). In the respect of the component elements in biochar, H, N and O element contents decrease, whereas C element content increases with increase of the pyrolysis temperature [44]. In addition, the aromatic property and hydrophobicity of biochar rise, and the polarity and hydrophilicity drop in terms of the trend of O/C, H/C and (O+N)/C with increase of the pyrolysis temperature [45]. Comparing with BC300, BET surface area, t -pLot surface area, t -pLot micropore area, and t -pLot micropore volume for BC600 increase by 34, 23, 40 and 42 times, respectively, indicating that increasing the pyrolysis temperature is conducive to increase the specific surface area of biochar and to form more mesoporous and microporous structures. Similarly, the Barrett–Joyner–Halenda average pore width and the BET average pore diameter for BC600 decrease based on those of BC300, showing that increase of pyrolysis temperature can lead to the collapse of larger size pores in biochar [46]. In summary, biochars have the main structural particularities such as high carbon content, porous and strong adsorption capacity.

SEM images of BC300 and BC600 are shown in Fig. 1. As can be seen, the biochar samples have irregularly strip structure with obvious pores. The surface of BC300 has abundant mesopores, which are arranged neatly, resulting from a mass of ash on the biochar surface being removed in the pickling process, making the surface of BC300 smooth and free of disorderly structure. Compared with BC300, BC600 has thinner tube wall, clearer pore structure, and smoother surface with increase of the pyrolysis temperature [47]. These results manifest that the pyrolysis temperature is a critical factor that affects the structure of biochar, which is consistent with the characterization results of pore structure and specific surface area.

Table 2
Primary physico-chemical properties of biochars

Biochar	pH ^a	pH ^b	Yield (%)	Ash (%)	Element content (%)				Atomic ratio		
					C	H	O	N	O/C	H/C	(O+N)/C
BC300	9.58	3.69	21.34	6.33	67.77	3.62	20.79	1.49	0.31	0.05	0.33
BC600	10.52	3.64	13.26	6.39	77.04	2.03	13.34	1.20	0.17	0.03	0.19
Biochar	SA _{BET} ^c (m ² /g)		SA _{t-pLot} ^d (m ² /g)		MA _{t-pLot} ^e (m ² /g)		MV _{t-pLot} ^f (cm ³ /g)		PW _{BH} ^g (Å)		PD _{BET} ^h (Å)
BC300	10.11		3.77		6.35		3.26 × 10 ⁻³		1.38 × 10 ²		15.23
BC600	3.48 × 10 ²		89.7		2.58 × 10 ²		1.39 × 10 ⁻¹		34.89		6.09

Notes: ^abefore pickling; ^bafter pickling; ^cBET surface area; ^d t -pLot surface area; ^e t -pLot micropore area; ^f t -pLot micropore volume; ^gBarrett–Joyner–Halenda average pore width; ^hBET average pore diameter.

The XPS spectra of biochar samples are shown in Fig. 2a. As can be seen, the biochars are mainly composed of C, N and O elements, and their corresponding binding energies are about 284, 401 and 531 eV, respectively.

The FTIR spectra of BC300 and BC600 are shown in Fig. 2b. The primary peaks can be assigned as follows: (a) the peak at 3,420.3 cm^{-1} is the stretching frequency of $-\text{OH}$; (b) the peaks at 2,983.1 and 2,830.1 cm^{-1} are aliphatic $-\text{CH}_2-$ and aromatic $-\text{CH}_2-$, respectively; (c) the peak at 2,359.5 cm^{-1} is the characteristic of $-\text{CH}$ or $-\text{OH}$ of the stretching vibration; (d) the peak at 1,603.4 cm^{-1} is the $\text{C}=\text{C}$ or $\text{C}=\text{O}$ of the aromatic ring; (e) the peaks at about 1,006.8 and 1,180.5 cm^{-1} are the $\text{C}-\text{O}$; (f) the peak at 792.1 cm^{-1} can be formed by the $\text{C}-\text{H}$ plane vibration and the stretching vibration of $\text{Si}-\text{O}-\text{Si}$. In general, the surface of BC300 and BC600 has a large number of $-\text{OH}$, $\text{C}=\text{C}$, and aromatic functional groups [48].

3.2. Adsorption of CPs

The equilibrium q_e values of CPs on BC300 and BC600 are listed in Table 3. As can be seen, the q_e values of BC600 on PHE, 4-CP, and 2,4-DCP were all higher than those of BC300 in the SCS, indicating that BC600 had a greater adsorption capacity than BC300. In fact, the experimental results were consistent with the preceding characterization results of pore structure, specific surface area, and SEM, that is, BC600 had a greater adsorption effect for CPs than BC300, so BC600 was selected as an adsorbent for follow-up experiments.

3.2.1. Effect of initial pH value

As Fig. 3. shows, the effect of initial pH on q_e of the CPs on BC600 in the MCS resembles that in the SCS. At $\text{pH} < 9$,

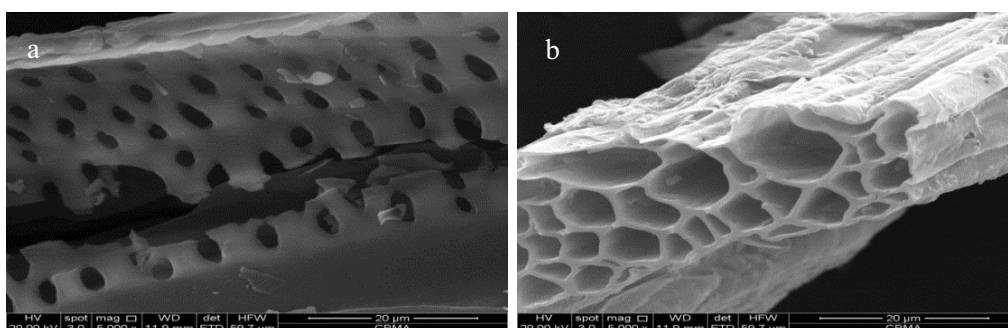


Fig. 1. Scanning electron microscopy images of (a) BC300 $\times 5\text{k}$ and (b) BC600 $\times 5\text{k}$.

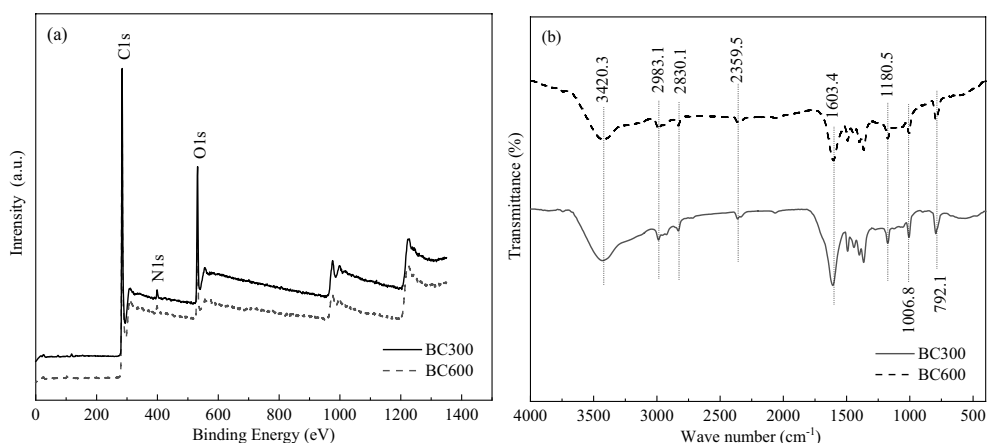


Fig. 2. (a) X-ray photoelectron spectra of BC300 and BC600 and (b) Fourier-transform infrared spectra of BC300 and BC600.

Table 3
Equilibrium q_e values for chlorophenols on BC300 and BC600 in single component system

	BC300			BC600		
	Phenol	4-Chlorophenol	2,4-Dichlorophenol	Phenol	4-Chlorophenol	2,4-Dichlorophenol
q_e^a (mg/g)	9.37	22.89	24.75	29.32	33.71	35.47
q_e^b (mg/g)	9.98	23.76	25.46	30.17	33.87	35.62

Notes: ^aAdsorption capacity of each of the chlorophenols fitted by pseudo-first-order kinetic model; ^bAdsorption capacity of each of the chlorophenols fitted by pseudo-second-order kinetic model.

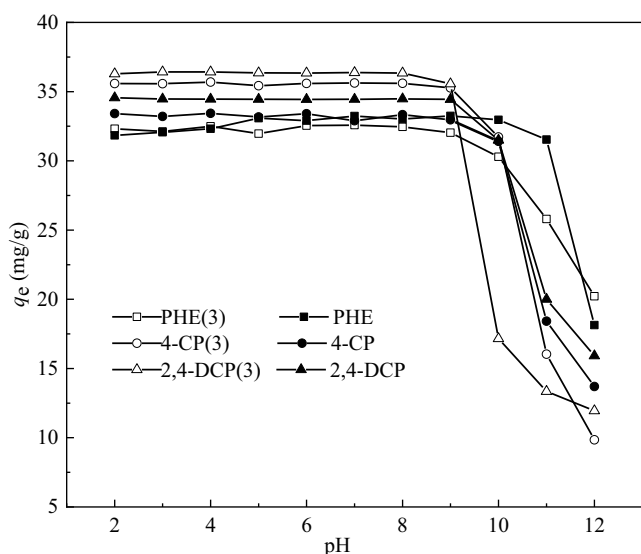


Fig. 3. Effect of initial pH on adsorption of chlorophenols on BC600 in the single component system and multi-component system. Note: “(3)” in the legend refer to co-existing phenol, 4-chlorophenol, and 2,4-dichlorophenol in the multi-component system.

the q_e values almost unchanged with the increase of the pH values both in the SCS and in the MCS, indicating that the pH has a little effect on the adsorption process CPs on BC600 under lower pH values. This may be because each of the CPs exists in a molecular form when the pH value of the solution is less than corresponding to its own pKa value. In acidic solution, the CPs can be protonated. The protonated CPs are easily adsorbed by BC600 via hydrogen-bond interaction between CPs and BC600 [49]. At $\text{pH} > 9$, however, the q_e values of CPs on BC600 decrease rapidly with the increase of the pH values of the solution. It can be seen that $\text{pH} = 9$ is the optimal value of this parameter. As Table 1 shows, the pKa value for PHE, 4-CP, and 2,4-DCP is 9.89, 9.70 and 7.89, respectively, accounting for when the pH value is greater than the corresponding to own pKa of each of the CPs, the acidic functional groups (e.g., $-\text{COOH}$, $-\text{OH}$) on the surface of the BC600 dissociate to form $-\text{COO}^-$ or $-\text{O}^-$ anions, which weakens the hydrogen bonding between BC600 and CPs. Furthermore, under alkaline condition, electrostatic repulsion between OH^- ions of the solution and the preceding anions also can reduce the adsorption capacity of CPs on BC600 [50]. At the same time, the q_e value in the SCS is greater than that in the MCS, indicating that the co-existing CPs in the MCS can inhibit the adsorption of each of CPs on BC600, this rule is consistent with the results of adsorption kinetics and isotherm.

3.2.2. Adsorption kinetics

Fig. 4. shows the trend of the adsorption of PHE, 4-CP, and 2,4-DCP on BC600 in the SCS and MCS with contact time. The q_t values increased rapidly at the starting stage, then gradually became slow, and finally reached equilibrium due to a lot of adsorption sites existed on the biochar surface at the starting stage. Then the adsorption sites were

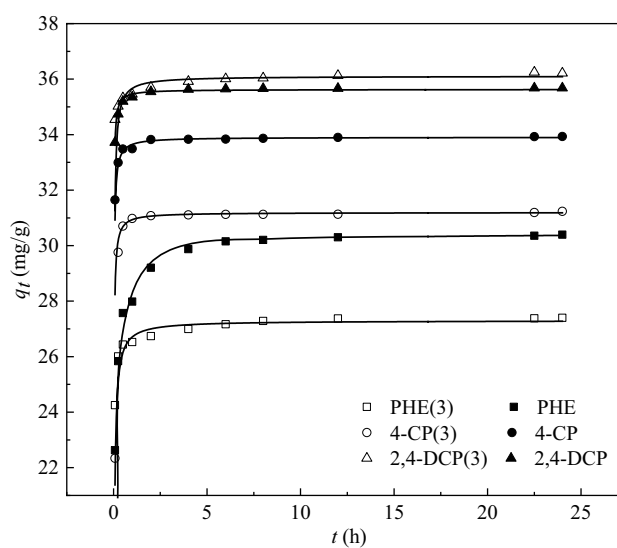


Fig. 4. Pseudo-second-order kinetic model fitting curve. Note: “(3)” in the legend refer to co-existing phenol, 4-chlorophenol, and 2,4-dichlorophenol in the multi-component system.

occupied by adsorbate in the later stage, resulting in the remaining adsorption sites no longer were occupied by CPs, so the adsorption gradually reached equilibrium [51].

The adsorption kinetic models are commonly applied to investigate the adsorption behavior and mechanisms. Here, the experimental data were fitted by pseudo-first-order kinetic, pseudo-second-order kinetic, and intraparticle diffusion models, respectively [listed in Eqs. (2)–(4)]. The fitted parameters are shown in Table 4. Compared with the pseudo-first-order model and the intraparticle diffusion model, the pseudo-second-order model fitted the experimental data better based on the higher correlation coefficient (R^2) and theory maximum adsorption capacity, q_e , approaching nearly to its experimental value, revealing that the adsorption of CPs onto two biochars followed the pseudo-second-order model law [52]. The fitted curves of the pseudo-second-order kinetic model are shown in Fig. 4.

Pseudo-first-order kinetic model:

$$q_t = q_e \left(1 - e^{-k_1 t}\right) \quad (2)$$

Pseudo-second-order kinetic model:

$$q_t = \frac{q_e^2 k_2 t}{1 + q_e k_2 t} \quad (3)$$

Intraparticle diffusion model:

$$q_t = k_d t^{1/2} + c_i \quad (4)$$

where q_t is the adsorption capacity at a given time (mg/g), q_e is the equilibrium adsorption capacity at the equilibrium time (mg/g), t is the contact time (h), c_i is the intercept of the intraparticle diffusion model, and k_1 (h^{-1}), k_2 ($\text{g}/(\text{mg}\cdot\text{h})$), and k_d ($\text{mg}/(\text{g}\cdot\text{h}^{1/2})$) are the rate constants of pseudo-first-

order kinetic model, pseudo-second-order kinetic model, and intraparticle diffusion model, respectively.

According to the fitting parameters of intraparticle diffusion model in Table 4, adsorption process is divided into two stages both in the SCS and MCS. The k_{d1} and k_{d2} are the intraparticle diffusion model rate constants which refer to the ease degree of diffusion of the pollutants within the adsorbent, that is, the higher the k_{d1} and k_{d2} , the easier the diffusion of the pollutants within the adsorbent [53]. It can be known from the preceding FTIR characterization in Fig. 2b. that many –OH groups exist on the BC600. They can form hydrogen bonding with the –OH group of CPs. The hydrogen bonding, which is a stronger induced dipole-induced dipole attractive forces, can help adsorb CPs better on biochar [54]. Besides, the order of adsorption capacity for CPs on the BC600 is 2,4-DCP > 4-CP > PHE. Obviously, this sequence is related to the number of chlorine atom in CPs. This is because the structure of PHE, 4-CP, and 2,4-DCP are similar, containing a benzene ring and a hydroxy group in their molecules, but the number of chlorine atoms is different. It is well known that the adsorption of CPs on biochar involves the formation of electron donor-acceptor complexes where the benzene ring of biochar bears electron rich region, acting as π -electron donors and the aromatic ring of CPs has electron poor region, serving as a π -electron acceptor due to the chlorine of CPs is a strong electron-withdrawing group, accounting for the higher adsorption capacity of 2,4-DCP than PHE and 4-CP [55]. Of them, 2,4-DCP contains the highest number of chlorine atoms, its adsorption capacity is the highest, whereas PHE has no chlorine atom, its adsorption capacity is the least. For 4-CP with a single chlorine atom, its adsorption is the middle between 2,4-DCP and PHE. These results showed that the adsorption of CPs on biochar is related to the number of chlorine atoms in the CPs, that is, the more the number of chlorine atoms, the more easily they are adsorbed on biochar.

3.2.3. Adsorption isotherms

Fig. 5. shows the effect of different equilibrium concentrations of pollutants on the adsorption of CPs on BC600 in the SCS and MCS. As can be seen, the q_e increased with the increase of the c_e and the sequence of adsorption of CPs on BC600 is 2,4-DCP > 4-CP > PHE, which was consistent with adsorption kinetics, both in the SCS and MCS. However, difference between both systems was observed. The q_e in the MCS was lower than that in the SCS, indicating that co-existing CPs in the MCS can hinder the adsorption of each of CPs on BC600.

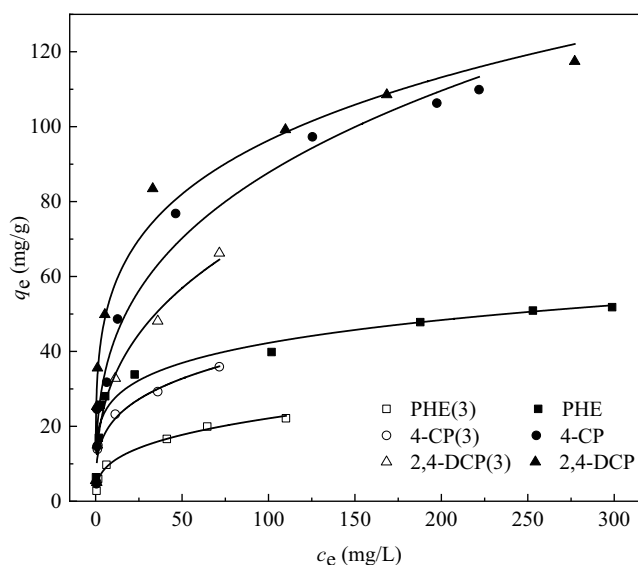


Fig. 5. Freundlich isotherm model fitting curve. Note: “(3)” in the legend refer to co-existing phenol, 4-chlorophenol, and 2,4-dichlorophenol in the multi-component system.

Table 4

Adsorption kinetic fitting parameters of chlorophenols on BC600 in the single component system and multi-component system

Chlorophenols	System	Pseudo-first-order kinetic model			Pseudo-second-order kinetic model		
		q_e (mg/g)	k_1 (h ⁻¹)	R^2	q_e (mg/g)	k_2 [g/(mg·h)]	R^2
Phenol	SCS	29.32	12.00	0.850	30.17	0.75	0.985
	MCS	26.93	29.41	0.761	28.16	3.66	0.943
4-Chlorophenol	SCS	33.71	37.02	0.827	33.87	5.11	0.986
	MCS	31.01	19.14	0.899	32.54	6.01	0.938
2,4-Dichlorophenol	SCS	35.47	15.91	0.770	35.62	5.87	0.973
	MCS	35.80	38.55	0.687	36.04	7.40	0.963
Chlorophenols	System	Intraparticle diffusion model					
		k_{d1} [g/(mg·h ^{1/2})]	c_1 (mg/g)	R^2	k_{d2} [g/(mg·h ^{1/2})]	c_2 (mg/g)	R^2
Phenol	SCS	10.95	18.43	0.749	0.27	29.21	0.661
	MCS	2.96	23.96	0.726	0.16	26.68	0.767
4-Chlorophenol	SCS	2.45	31.37	0.614	0.03	33.76	0.949
	MCS	10.92	21.64	0.661	0.03	31.02	0.912
2,4-Dichlorophenol	SCS	2.12	33.38	0.771	0.03	35.38	0.646
	MCS	1.25	34.31	0.898	0.13	35.92	0.889

Table 5
Adsorption isotherm fitting parameters of chlorophenols on BC600 in the single component system and multi-component system

Chlorophenols	System	Langmuir			Freundlich			
		q_m (mg/g)	K_L	R^2	K_F	n	R^2	
Phenol	SCS	47.24	0.29	0.908	17.22	3.13	0.950	
	MCS	21.64	0.16	0.945	5.06	3.12	0.987	
4-Chlorophenol	SCS	129.89	0.06	0.839	20.75	3.08	0.913	
	MCS	32.47	0.50	0.877	11.57	3.76	0.934	
2,4-Dichlorophenol	SCS	105.09	0.25	0.939	33.55	4.43	0.972	
	MCS	96.92	0.13	0.969	13.83	1.72	0.990	

Chlorophenols	System	Sips			Langmuir–Freundlich				
		q_m (mg/g)	K_S	n	R^2	q_m (mg/g)	K_L	n	R^2
Phenol	SCS	42.26	3.85	1.87	0.829	62.91	0.32	0.44	0.966
	MCS	21.65	1.08	6.98	0.927	43.02	0.12	0.46	0.991
4-Chlorophenol	SCS	132.90	4.55	4.21	0.827	121.03	0.07	0.47	0.983
	MCS	32.47	5.72	7.62	0.836	60.85	0.23	0.41	0.938
2,4-Dichlorophenol	SCS	105.09	1.45	5.71	0.927	145.09	0.26	0.45	0.995
	MCS	96.26	21.99	9.14	0.959	96.48	0.14	0.58	0.983

The adsorption isotherms experiment data were fitted by Langmuir, Freundlich, Sips, and Langmuir–Freundlich isotherm models, respectively, as followed.

Langmuir model:

$$q_e = \frac{q_m K_L c_e}{1 + K_L c_e} \quad (5)$$

Freundlich model:

$$q_e = K_F c_e^{1/n} \quad (6)$$

Sips model:

$$q_e = \frac{q_m K_S c_e^{1/n}}{1 + K_S c_e^{1/n}} \quad (7)$$

Langmuir–Freundlich model:

$$q_e = \frac{q_m K_L c_e^n}{1 + K_L c_e^n} \quad (8)$$

where c_e is the equilibrium concentration of CPs (mg/L), q_e is the adsorption capacity corresponding to c_e (mg/g), q_m is the maximum adsorption capacity (mg/g), $1/n$ is the non-uniformity coefficient of Freundlich model, K_L is constant of Langmuir or Langmuir–Freundlich model, and K_F and K_S is constant of Freundlich, and Sips model, respectively.

Adsorption isotherm fitting parameters of CPs on BC600 in the SCS and MCS are listed in Table 5. As the table showed, the R^2 values of Langmuir–Freundlich isotherm model were the highest, indicating that the adsorption process of CPs on BC600 may exist multi-molecular layer adsorption. By way of contrast, Langmuir model parameter K_L values are

all less than 1, reflecting that the adsorption process may also exist a single molecular layer adsorption [56]. So the adsorption of CPs on biochar not only exist single molecular layer adsorption, but also may do multi-molecular layer adsorption [57]. In addition, the q_m value fitted by each of Langmuir, Sips, and Langmuir–Freundlich isotherm models increases with the increase of the c_e values, and the q_m in the MCS is lower than that of in the SCS, indicating that there is a clearly competitive adsorption for sites on BC600 between the CPs in the MCS, that is, the co-existing CPs in the MCS can inhibit the adsorption of each of CPs on BC600. The competitive adsorption occurs due to the electrostatic repulsion of the CPs [58].

4. Conclusions

BC600, the biochar obtained at the higher hydrolyzed temperature, has rich carbon constitution, greater special surface area, more developed porous structure and much more aromaticity than BC300, the biochar produced at the lower hydrolyzed temperature. According to these structure features, it can be predicted that BC600 bears better adsorption capacity for CPs compared with BC300. The results on initial pH influence, adsorption kinetic and adsorption isotherm indicated that the adsorption regularities of CPs on biochar in the MCS are almost same as those in the SCS. The adsorption kinetic process of CPs on biochar is well described by the pseudo-second-order model. The adsorption isotherm followed better the Langmuir–Freundlich model. The initial pH of solution is a critical factor influencing adsorption process, that is, at $\text{pH} < 9$, the q_e values of CPs on biochar are relatively stable, whereas at $\text{pH} > 9$, the q_e values of the CPs decrease rapidly. Notably, (1) the q_e values of PHE, 4-CP and 2,4-DCP in the MCS (43.02, 60.82 and 96.48 mg/g) are lower than those in the SCS (62.91, 121.03 and 145.09 mg/g), indicating that the co-existing CPs in the MCS can inhibit the

adsorption of any single substance of CPs on biochar; (2) the q_e values of CPs on BC600 are related tightly to the number of chlorine atoms in CPs, that is, the more chlorine atoms in CPs, the easier it is adsorbed by BC600.

Acknowledgements

This work was supported by the National Natural Science Foundation of China (22166022), the Plan Project of science and Technology of Gansu Province (20JR2RA002), and the Science and Technology Innovation Project of Lanzhou Jiaotong University (DXS 2022-035).

References

- [1] B.N. Cemre, M. Bekbolet, Role of emerging contaminants on solar photocatalytic treatment of organic matter in reverse osmosis concentrate, *Catal. Today*, 326 (2019) 101–107.
- [2] L.M.M. Machado, S.F. Lütke, D. Perondi, M. Godinho, M.L.S. Oliveira, G.C. Collazzo, G.L. Dotto, Treatment of effluents containing 2-chlorophenol by adsorption onto chemically and physically activated biochars, *J. Environ. Chem. Eng.*, 8 (2020) 104473, doi: 10.1016/j.jece.2020.104473.
- [3] Z. Ghahghaey, M. Hekmati, G.M. Darvish, Theoretical investigation of phenol adsorption on functionalized graphene using DFT calculations for effective removal of organic contaminants from wastewater, *J. Mol. Liq.*, 324 (2021) 114777, doi: 10.1016/j.molliq.2020.114777.
- [4] Z.H. Chen, J. Yao, B. Ma, B. Liu, J. Kim, H. Li, X.Z. Zhu, C.C. Zhao, M. Amde, A robust biocatalyst based on laccase immobilized superparamagnetic $\text{Fe}_3\text{O}_4/\text{SiO}_2\text{-NH}_2$ nanoparticles and its application for degradation of chlorophenols, *Chemosphere*, 291 (2022) 132727, doi: 10.1016/j.chemosphere.2021.132727.
- [5] Y.X. Zhao, X.J. Qiu, Z.H. Ma, C.L. Zhao, Z.R. Li, S.Y. Zhai, Fabrication of Pd/sludge-biochar electrode with high electrochemical activity on reductive degradation of 4-chlorophenol in wastewater, *Environ. Res.*, 209 (2022) 112740, doi: 10.1016/j.envres.2022.112740.
- [6] M.Y. Zhu, J. Lu, L.C. Dong, S.H. Hu, S.H. Peng, C.Z. Zhu, Photochemical transformations of 2,6-dichlorophenol and 2-chlorophenol with superoxide ions in the atmospheric aqueous phase, *J. Mol. Struct.*, 1261 (2022) 132910, doi: 10.1016/j.molstruc.2022.132910.
- [7] W. Tirler, A. Basso, Resembling a “natural formation pattern” of chlorinated dibenzo-p-dioxins by varying the experimental conditions of hydrothermal carbonization, *Chemosphere*, 93 (2013) 1464–1470.
- [8] M. Chen, P. Xu, G.M. Zeng, C.P. Yang, D.L. Huang, J.C. Zhang, Bioremediation of soils contaminated with polycyclic aromatic hydrocarbons, petroleum, pesticides, chlorophenols and heavy metals by composting: applications, microbes and future research needs, *Biotechnol. Adv.*, 33 (2015) 745–755.
- [9] M. Czaplicka, Sources and transformations of chlorophenols in the natural environment, *Sci. Total Environ.*, 322 (2004) 21–39.
- [10] V. Sivanantham, P.L. Narayana, K.J. Hyeong, P. Parreddy, V. Sangeetha, M. Kyoung-Seok, K.H. In, H.K. Sung, N.S. Reddy, Modeling and optimization of chlorophenol rejection for spiral wound reverse osmosis membrane modules, *Chemosphere*, 268 (2021) 129345, doi: 10.1016/j.chemosphere.2020.129345.
- [11] V. Vaiano, M. Matarangolo, J.J. Murcia, H. Rojas, J.A. Navío, M.C. Hidalgo, Enhanced photocatalytic removal of phenol from aqueous solutions using ZnO modified with Ag, *Appl. Catal., B*, 225 (2018) 197–206.
- [12] S. Ahmed, M.G. Rasul, W.N. Martens, R. Brown, M.A. Hashib, Heterogeneous photocatalytic degradation of phenols in wastewater: a review on current status and developments, *Desalination*, 261 (2010) 3–18.
- [13] D. Maity, P. Kundu, S. Adhikari (Nee Pramanik), Isolation and characterization of 4-chlorophenol degrading bacterial strain from pharmaceutical xenobiotic compounds contaminated soil using enrichment technique, *J. Indian Chem. Soc.*, 99 (2022) 100336, doi: 10.1016/j.jics.2021.100336.
- [14] Z.Y. Zhao, J.N. Zhang, J. Yao, S.J. You, Electrochemical removal of 4-chlorophenol in water using a porous Magnéli-phase (Ti_4O_7) electrode, *Environ. Res.*, 210 (2022) 113004, doi: 10.1016/j.envres.2022.113004.
- [15] N. Dominguez-Morueco, M. Carvalho, J. Sierra, M. Schuhmacher, J.L. Domingo, N. Ratola, M. Nadal, Multi-component determination of atmospheric semi-volatile organic compounds in soils and vegetation from Tarragona County, Catalonia, Spain, *Sci. Total Environ.*, 631–632 (2018) 1138–1152.
- [16] L. Bulgariu, L.B. Escudero, O.S. Bello, M. Iqbal, J. Nisar, K.A. Adegoke, F. Alakhras, M. Kornaros, I. Anastopoulos, The utilization of leaf-based adsorbents for dyes removal: a review, *J. Mol. Liq.*, 276 (2019) 728–747.
- [17] G. Song, P. Su, Q.Z. Zhang, X.C. Wang, M.H. Zhou, Revisiting UV/sulfite exposed to air: a redox process for reductive dechlorination and oxidative mineralization, *Sci. Total Environ.*, 859 (2023) 160246, doi: 10.1016/j.scitotenv.2022.160246.
- [18] S. Praveen, J. Jegan, T.B. Pushpa, R. Gokulan, L. Bulgariu, Biochar for removal of dyes in contaminated water: an overview, *Biochar*, 4 (2022) 10, doi: 10.1007/s42773-022-00131-8.
- [19] J.J. Wei, D.H. Ma, X.R. Ma, Q. Sheng, X.Y. Sun, J.S. Li, X.D. Liu, J.Y. Shen, M. Zheng, L.J. Wang, New insight into increased toxicity during ozonation of chlorophenol: the significant contribution of oxidizing intermediates, *Sci. Total Environ.*, 769 (2021) 144569, doi: 10.1016/j.scitotenv.2020.144569.
- [20] Y.E. Dolaksiz, F. Temel, M. Tabakci, Adsorption of phenolic compounds onto calix[4]arene-bonded silica gels from aqueous solutions, *React. Funct. Polym.*, 126 (2018) 27–35.
- [21] G.J. Cai, Z.-l. Ye, Concentration-dependent adsorption behaviors and mechanisms for ammonium and phosphate removal by optimized Mg-impregnated biochar, *J. Cleaner Prod.*, 349 (2022) 131453, doi: 10.1016/j.jclepro.2022.131453.
- [22] X.Y. Zhang, X.Y. Wang, J.Q. Meng, Y.Q. Liu, M. Ren, Y.H. Guo, Y.X. Yang, Robust Z-scheme $\text{g-C}_3\text{N}_4/\text{WO}_3$ heterojunction photocatalysts with morphology control of WO_3 for efficient degradation of phenolic pollutants, *Sep. Purif. Technol.*, 255 (2021) 117693, doi: 10.1016/j.seppur.2020.117693.
- [23] B. Zhang, R.G. Zhao, D.J. Sun, Y. Li, T. Wu, Sustainable fabrication of graphene oxide/manganese oxide composites for removing phenolic compounds by adsorption-oxidation process, *J. Cleaner Prod.*, 215 (2019) 165–174.
- [24] M. Ahmad, A.U. Rajapaksha, J.E. Lim, M. Zhang, N. Bolan, D. Mohan, M. Vithanage, S.S. Lee, Y.S. Ok, Biochar as a sorbent for contaminant management in soil and water: a review, *Chemosphere*, 99 (2014) 19–33.
- [25] Y.J. Dai, J.J. Li, D.X. Shan, Adsorption of tetracycline in aqueous solution by biochar derived from waste *Auricularia auricula* dregs, *Chemosphere*, 238 (2020) 124432, doi: 10.1016/j.chemosphere.2019.124432.
- [26] S.S. Mao, T. Shen, T. Han, F. Ding, Q. Zhao, M. Gao, Adsorption and co-adsorption of chlorophenols and Cr(VI) by functional organo-vermiculite: experiment and theoretical calculation, *Sep. Purif. Technol.*, 277 (2021) 119638, doi: 10.1016/j.seppur.2021.119638.
- [27] X.W. Cao, Z.F. Meng, E. Song, X.X. Sun, X.L. Hu, W.B. Li, Z. Liu, S. Gao, B. Song, Co-adsorption capabilities and mechanisms of bentonite enhanced sludge biochar for de-risking norfloxacin and Cu^{2+} contaminated water, *Chemosphere*, 299 (2022) 134414, doi: 10.1016/j.chemosphere.2022.134414.
- [28] P.T. Hernandes, D.S.P. Franco, J. Georjina, N.P.G. Salau, G.L. Dotto, Investigation of biochar from *Cedrella fissilis* applied to the adsorption of atrazine herbicide from an aqueous medium, *J. Environ. Chem. Eng.*, 10 (2022) 107408, doi: 10.1016/j.jece.2022.107408.
- [29] T.C.P. Tran, T.P. Nguyen, T.T. Nguyen, P.C. Le, Q.B. Tran, X.C. Nguyen, Equilibrium single and co-adsorption of nutrients from aqueous solution onto aluminium-modified biochar, *Case Stud. Chem. Environ. Eng.*, 5 (2022) 100181, doi: 10.1016/j.cscee.2022.100181.
- [30] N. Zhao, C.F. Zhao, Y.Z. Lv, W.F. Zhang, Y.G. Du, Z.P. Hao, J. Zhang, Adsorption and coadsorption mechanisms of

- Cr(VI) and organic contaminants on H_3PO_4 treated biochar, *Chemosphere*, 186 (2017) 422–429.
- [31] S. Larous, A.-H. Meniai, The use of sawdust as by product adsorbent of organic pollutant from wastewater: adsorption of phenol, *Energy Procedia*, 18 (2012) 905–914.
- [32] T.T.H. Chu, M.V. Nguyen, Improved Cr(VI) adsorption performance in wastewater and groundwater by synthesized magnetic adsorbent derived from Fe_3O_4 loaded corn straw biochar, *Environ. Res.*, 216 (2023) 114764, doi: 10.1016/j.envres.2022.114764.
- [33] C.T. do Nascimento, M.G.A. Vieira, F.B. Scheufele, F. Palú, E.A. da Silva, C.E. Borba, Adsorption of atrazine from aqueous systems on chemically activated biochar produced from corn straw, *J. Environ. Chem. Eng.*, 10 (2022) 107039, doi: 10.1016/j.jece.2021.107039.
- [34] F. Wang, L. Li, J.B. Iqbal, Z.R. Yang, Y.P. Du, Preparation of magnetic chitosan corn straw biochar and its application in adsorption of amaranth dye in aqueous solution, *Int. J. Biol. Macromol.*, 199 (2022) 234–242.
- [35] Y.Z. Zhang, S.X. Liang, R. He, J. Zhao, J.H. Lv, W. Kang, J. Zhang, Enhanced adsorption and degradation of antibiotics by doping corn cob biochar/PMS with heteroatoms at different preparation temperatures: mechanism, pathway, and relative contribution of reactive oxygen species, *J. Water Process Eng.*, 46 (2022) 102626, doi: 10.1016/j.jwpe.2022.102626.
- [36] Q.A. Binh, H.-H. Nguyen, Investigation the isotherm and kinetics of adsorption mechanism of herbicide 2,4-dichlorophenoxyacetic acid (2,4-D) on corn cob biochar, *Bioresour. Technol. Rep.*, 11 (2020) 100520, doi: 10.1016/j.biteb.2020.100520.
- [37] E. Taheri, A. Fatehizadeh, E.C. Lima, M. Rezakazemi, High surface area acid-treated biochar from pomegranate husk for 2,4-dichlorophenol adsorption from aqueous solution, *Chemosphere*, 295 (2022) 133850, doi: 10.1016/j.chemosphere.2022.133850.
- [38] Z. Li, M. Li, Z.Y. Wang, X. Liu, Co-adsorption of Cu(II) and tylosin/sulfamethoxazole on biochar stabilized by nano-hydroxyapatite in aqueous environment, *Chem. Eng. J.*, 381 (2020) 122785, doi: 10.1016/j.cej.2019.122785.
- [39] Q. Gan, H.J. Hou, S. Liang, J.J. Qiu, S.Y. Tao, L. Yang, W.B. Yu, K.K. Xiao, B.C. Liu, J.P. Hu, Y.F. Wang, J.K. Yang, Sludge-derived biochar with multivalent iron as an efficient Fenton catalyst for degradation of 4-chlorophenol, *Sci. Total Environ.*, 725 (2020) 138299, doi: 10.1016/j.scitotenv.2020.138299.
- [40] X. Jiang, X. Ye, J. Xiao, W.H. Zhang, R. Qiu, The effect of persistent free radicals in sludge derived biochar on p-chlorophenol removal, *Chemosphere*, 297 (2022) 134218, doi: 10.1016/j.chemosphere.2022.134218.
- [41] F.-X. Dong, L. Yan, X.-H. Zhou, S.-T. Huang, J.-Y. Liang, W.-X. Zhang, Z.-W. Guo, P.-R. Guo, W. Qian, L.-J. Kong, W. Chu, Z.-H. Diao, Simultaneous adsorption of Cr(VI) and phenol by biochar-based iron oxide composites in water: performance, kinetics and mechanism, *J. Hazard. Mater.*, 416 (2021) 125930, doi: 10.1016/j.jhazmat.2021.125930.
- [42] R. Singh, R.K. Dutta, D.V. Naik, A. Ray, P.K. Kanaujia, High surface area *Eucalyptus* wood biochar for the removal of phenol from petroleum refinery wastewater, *Environ. Challenges*, 5 (2021) 100353, doi: 10.1016/j.envc.2021.100353.
- [43] T. Zhang, L.C. Zheng, H.J. Yu, J.J. Ren, D. Peng, L.J. Zhang, P.P. Meng, Multiple adsorption systems and electron-scale insights into the high efficiency co-adsorption of a novel assembled cellulose via experiments and DFT calculations, *J. Hazard. Mater.*, 416 (2021) 125748, doi: 10.1016/j.jhazmat.2021.125748.
- [44] M.J. Ahmed, B.H. Hameed, Insights into the isotherm and kinetic models for the co-adsorption of pharmaceuticals in the absence and presence of metal ions: a review, *J. Environ. Manage.*, 252 (2019) 109617, doi: 10.1016/j.jenvman.2019.109617.
- [45] P.Y. Du, L. Xu, Z.J. Ke, J.X. Liu, T. Wang, S. Chen, M. Mei, J.P. Li, S.J. Zhu, A highly efficient biomass-based adsorbent fabricated by graft copolymerization: kinetics, isotherms, mechanism and co-adsorption investigations for cationic dye and heavy metal, *J. Colloid Interface Sci.*, 616 (2022) 12–22.
- [46] Z.H. Yin, Y.G. Liu, S.B. Liu, L.H. Jiang, X.F. Tan, G.M. Zeng, M.F. Li, S.J. Liu, S.R. Tian, Y. Fang, Activated magnetic biochar by one-step synthesis: enhanced adsorption and co-adsorption for 17 β -estradiol and copper, *Sci. Total Environ.*, 639 (2018) 1530–1542.
- [47] Y. Zhang, B. Cao, L.L. Zhao, L. Sun, Y. Gao, J.J. Li, F. Yang, Biochar-supported reduced graphene oxide composite for adsorption and co-adsorption of atrazine and lead ions, *Appl. Surf. Sci.*, 427 (2018) 147–155.
- [48] M. Karimi, M. Shirzad, J.A.C. Silva, A.E. Rodrigues, Biomass/biochar carbon materials for CO₂ capture and sequestration by cyclic adsorption processes: a review and prospects for future directions, *J. CO₂ Util.*, 57 (2022) 101890, doi: 10.1016/j.jcou.2022.101890.
- [49] G. Liu, H.R. Tang, J.J. Fan, Z.H. Xie, T.Y. He, R. Shi, B. Liao, Removal of 2,4,6-trichlorophenol from water by *Eupatorium adenophorum* biochar-loaded nano-iron/nickel, *Bioresour. Technol.*, 289 (2019) 121734, doi: 10.1016/j.biortech.2019.121734.
- [50] H. Li, S.Y. Li, L. Jin, Z. Lu, M.H. Xiang, C. Wang, W.B. Wang, J. Zhang, C.Y. Li, H.J. Xie, Activation of peroxydisulfate by magnetic Fe_3O_4 /biochar composites for the efficient degradation of 2,4,6-trichlorophenol: synergistic effect and mechanism, *J. Environ. Chem. Eng.*, 10 (2022) 107085, doi: 10.1016/j.jece.2021.107085.
- [51] D.L. Wei, C.F. Zhao, A. Khan, L. Sun, Y.F. Ji, Y.J. Ai, X.K. Wang, Sorption mechanism and dynamic behavior of graphene oxide as an effective adsorbent for the removal of chlorophenol based environmental-hormones: a DFT and MD simulation study, *Chem. Eng. J.*, 375 (2019) 121964, doi: 10.1016/j.cej.2019.121964.
- [52] P.S. Fabian, D.H. Lee, S.W. Shin, J.-H. Kang, Assessment of pyrene adsorption on biochars prepared from green infrastructure plants: toward a closed-loop recycling in managing toxic stormwater pollutants, *J. Water Process Eng.*, 48 (2022) 102929, doi: 10.1016/j.jwpe.2022.102929.
- [53] X.P. Yang, D. Jiang, X.X. Cheng, C. Yuan, S. Wang, Z.X. He, S. Esakkimuthu, Adsorption properties of seaweed-based biochar with the greenhouse gases (CO₂, CH₄, N₂O) through density functional theory (DFT), *Biomass Bioenergy*, 163 (2022) 106519, doi: 10.1016/j.biombioe.2022.106519.
- [54] Q. Xu, Q. Zhou, M.M. Pan, L.C. Dai, Interaction between chlortetracycline and calcium-rich biochar: enhanced removal by adsorption coupled with flocculation, *Chem. Eng. J.*, 382 (2020) 122705, doi: 10.1016/j.cej.2019.122705.
- [55] B. Okolo, C. Park, M.A. Keane, Interaction of phenol and chlorophenols with activated carbon and synthetic zeolites in aqueous media, *J. Colloid Interface Sci.*, 226 (2000) 308–317.
- [56] M.T. Sekulic, N. Boskovic, M. Milanovic, N.G. Letic, E. Gligoric, S. Pap, An insight into the adsorption of three emerging pharmaceutical contaminants on multifunctional carbonous adsorbent: mechanisms, modelling and metal co-adsorption, *J. Mol. Liq.*, 284 (2019) 372–382.
- [57] A. Tóth, A. Töröcsik, E. Tombác, K. László, Competitive adsorption of phenol and 3-chlorophenol on purified MWCNTs, *J. Colloid Interface Sci.*, 387 (2012) 244–249.
- [58] Y.J. Zhao, X.T. Liu, W.H. Li, K. Huang, H.Q. Shao, C. Qu, J.M. Liu, One-step synthesis of garlic peel derived biochar by concentrated sulfuric acid: enhanced adsorption capacities for Enrofloxacin and interfacial interaction mechanisms, *Chemosphere*, 290 (2022) 133263, doi: 10.1016/j.chemosphere.2021.133263.